

Communications

Graded Index Silicon Micromachined Lens Antenna: Enabling 36-dBi Gain and Circular Polarization at 500–750 GHz

Alireza Madannejad^{1b}, Mohammad Mehrabi Gohari^{1b}, Umer Shah^{1b}, and Joachim Oberhammer^{1b}

Abstract—This communication introduces a graded index (GRIN) Fresnel zone planar lens (FZPL) antenna operating with high gain in the 500–750-GHz frequency range. The main innovation involves achieving a gain of 35.9 dBi by incorporating a GRIN dielectric perforated disk. This perforated disk acts as a distributed spatial delay for beam focusing, ensuring gain improvement and circular polarization simultaneously without needing an extra polarizer. The antenna exhibits high efficiency, with an average radiation efficiency of -1.05 dB, achieved through the optimization of a modified FZPL for silicon-on-insulator (SOI) micromachining technology. The antenna maintains a return loss below -15 dB across the entire 500–750-GHz band, achieving a 40% fractional bandwidth, with circular polarization maintained and an axial ratio consistently below 2.8 dB. The fabricated chip, sized 12.18×12.18 mm with a thickness of $526 \mu\text{m}$, enhances practicality. The feeding arrangement involves a standard open waveguide, and direct mounting into a standard WM-380 waveguide flange is facilitated. This communication discusses the prototype's design, fabrication, and measurement, emphasizing the excellent agreement between the antenna's performance and simulated data.

Index Terms—Circularly polarized, graded index, silicon micromachining, terahertz (THz) antenna.

I. INTRODUCTION

The terahertz (THz) frequency range, spanning from 0.3 to 3 THz, has garnered increasing attention as a frontier for next-generation wireless communications and high-resolution imaging systems [1], [2]. These frequencies hold the potential to revolutionize applications requiring ultrahigh-speed data transmission and advanced sensing capabilities. However, one of the significant challenges in exploiting the THz band is the development of high-gain antennas that can overcome the inherent propagation losses and achieve the necessary transmission distances [3], [4], [5], [6], [7], [8]. For applications in the THz frequency range that demands high gain, lens antennas could be an ideal option. There are now two types of lenses in use: First, artificially created metal lenses with dispersion properties, and second, dielectric lenses. Based on the commercial milling process in [9], a metallic lens is proposed at 460 GHz with more than 27-dBi gain and only 21% fractional bandwidth (FBW). Dielectric lens antenna in the THz frequency can be classified into two types. First, the dielectric lens is based on the 3-D printing material [10], [11] to implement the graded index (GRIN) lenses. Second, the silicon-based lenses [12], [13], [14] are fabricated with microfabrication. The 3-D printing method is limited in the THz frequency because of the resolution accuracy of the 3-D printers and loss of the specific materials for printing [10], while silicon micromachining can provide precise dimensional control, smooth surface morphology, and

low loss properties. Furthermore, these technologies are compatible with Si-based integrated circuits (ICs) fabrication technology [15], [16], [17], [18]. At 550 GHz, a silicon lens is introduced in [19], capable of scanning beams with a gain exceeding 27 dBi. However, its bandwidth is constrained with only 18% FBW, and the fabrication process is intricate due to the requirement of a complex hemispherical structure for this design. Complex fabrication procedure for nonplanar antennas limits their implementation at THz frequency since the fabrication resolution is limited to provide desired curvature and edges for the nonplanar structures [19]. A planar lens antenna has been shown as an excellent alternative to the complex topology of spherical and high-volume lenses. Our previous work has been done in developing the planar lens at 750 GHz [8] with a simple fabrication process and novel elliptical Fresnel zone structure. This innovative approach guarantees the creation of a planar lens with highly efficient radiation, featuring a wideband and circular polarized property. However, the gain of this structure is capped at 25.7 dBi. In [8], an elliptical Fresnel zone planar lens (FZPL) antenna was introduced to enhance bandwidth while maintaining circular polarization, achieving a measured gain of 25.7 dBi. The elliptical shape improved bandwidth but reduced peak gain due to modified zone geometry. Conversely, this study uses a circular-zone FZPL, optimizing for maximum gain while retaining wideband operation. In an effort to enhance the gain of the FZPL antenna, the present study introduces a GRIN silicon dielectric perforated disk. This dielectric perforated disk serves the dual purpose of acting as a symmetrical polarizer and a phase compensator, building upon previous research findings.

This work presents a high-gain, circularly polarized lens antenna based on the modified planar Fresnel zones lens structure at THz frequency enabled by silicon micromachining. The primary innovation incorporates a GRIN dielectric perforated disk, functioning as a distributed spatial delay mechanism for precise beam focusing. This novel approach ensures simultaneous improvements in gain, aperture efficiency, and symmetrical circular polarization, eliminating the necessity for an additional polarizer. The modified FZPL reported here represents the first circular polarized high-gain antenna in the THz frequency with more than 31-dBi gain, enabled by silicon micromachining.

II. ANTENNA STRUCTURE AND DESIGN

The proposed antenna structure comprises two principal components: the Fresnel zone lens, characterized by a circular-shaped zone formed through the combination of dielectric and air, and the dielectric perforated disk, which is structured as a GRIN. The dielectric structure regulates delays at various locations, imparting the required phase shift for beam focusing and polarization control. Integrating both the components results in a wideband, high-gain, and circularly polarized antenna. Sections II-A–II-C provides a detailed examination of each component's design and integration.

A. Fresnel Zone Lens

FZPL antenna is desirable for high-gain applications due to its low profile, planar structure, and simple fabrication. Fig. 1 illustrates a

Received 17 September 2024; revised 24 March 2025; accepted 27 April 2025. Date of publication 12 May 2025; date of current version 6 August 2025. This work was supported by Swedish Foundation for Strategic Research under Grant CH119-0027. (Corresponding author: Alireza Madannejad.)

The authors are with the Department of Electrical Engineering, Division MST, Royal Institute of Technology, KTH, SE-100 44 Stockholm, Sweden (e-mail: madann@kth.se).

Digital Object Identifier 10.1109/TAP.2025.3567447

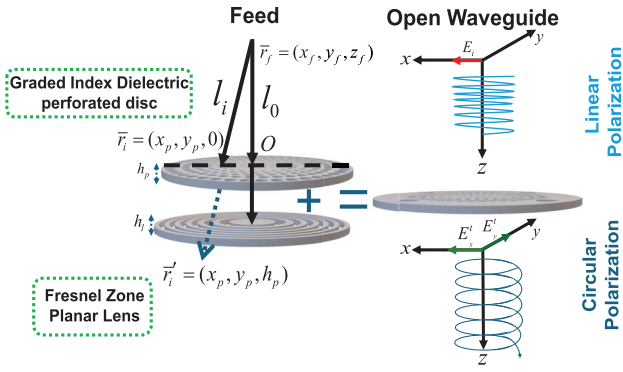


Fig. 1. Configuration of the proposed FZPL and dielectric perforated disk.

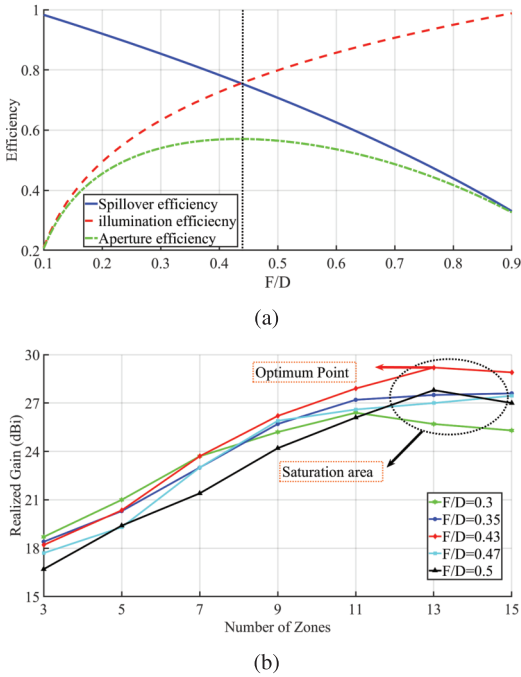


Fig. 2. Comparative simulation analysis of (a) spillover and illumination efficiency in FZPL and (b) investigating the tradeoff between focal point to lens size ratio (F/D), number of zones, and realized gain.

basic FZPL, consisting of dielectric zones with alternating air and dielectric materials. The outer radii of these zones are determined as discussed in [8]. The chosen material is silicon with $\epsilon_r = 11.9$ and a loss tangent of 0.000118 at 625 GHz. The focus-to-diameter (F/D) ratio is optimized at 0.43 for an open waveguide feed with 7.3-dBi gain to balance illumination and spillover efficiency, as shown in Fig. 2(a). Increasing the number of Fresnel zones enhances gain, but as Fig. 2(b) shows, beyond 13 zones, no further gain improvement occurs. As Fig. 2(b) shows, the gain saturates at 29 dBi with 13 zones and 12.18×12.18 mm, illustrating the fundamental size-gain tradeoff. Furthermore, the current antenna is 2.35 times larger in aperture area than the design in [8], which alone contributes 3.7 dB more gain. However, to further improve gain beyond this inherent size-based enhancement, we integrate a GRIN perforated disk to increase aperture efficiency by precisely controlling wave delays. This enables improved phase correction and more effective energy focusing. The total number of zones determines the antenna's gain. This design maximizes FZPL gain at 29 dBi with $N = 13$ zones. To surpass this limit, a practical approach is modifying ray delays by manipulating dielectric properties and altering the incident wave's wavenumber.

This strategy, implemented via a dielectric perforated disk, optimizes performance and enhances achievable gain.

B. Dielectric Perforated Disk

The spherical waves from the feed pass through various Fresnel zones and form a quasi-plane wave with a transmission phase shift of less than 180° . A modified Fresnel lens is proposed to improve the phase-correcting capability of FZPL, as shown in Fig. 1. Dielectric perforated disk is added to modify the spatial phase delay from the feed to the lens. As shown in Fig. 1, the lens radiates a focused beam along \hat{u} where

$$\hat{u} = \hat{x} \sin \theta_b \cos \varphi_b + \hat{y} \sin \theta_b \sin \varphi_b + \hat{z} \cos \theta_b \quad (1)$$

where (θ_b, φ_b) is the main beam direction of the lens. The required phase to compensate for the transmission of rays through the lens can be expressed using geometric optics and given as

$$\varphi_i = k_0 (|\vec{r}_i - \vec{r}_f| - \vec{r}'_i \cdot \hat{u} - l_0) \quad (2)$$

where k_0 is the free-space wavenumber, and \vec{r}_i and \vec{r}'_i are the position vectors of the bottom and top surfaces of the i th dielectric perforated disk, respectively. The center of the coordinate system O is set as the reference point, the distance from the phase center of the feed, and the reference point. Considering the broadside beam (i.e., $\theta_b = 0$, $\varphi_b = 0$), (1) can be written as

$$\varphi_i = k_0 \left(\sqrt{(x_f - x_i)^2 + (y_f - y_i)^2 + z_f^2} - h_p - l_0 \right). \quad (3)$$

The realized transmission shift of the dielectric perforated disk depends on the transmission and reflection from both the ends. The transmission coefficient of the modified Fresnel lens can be derived using the matching and propagation matrices and given by

$$T_{x/y} = \frac{\tau_{1,x/y} \tau_{2,x/y} e^{-jk_{x/y} h_p}}{1 + \rho_{1,x/y} \rho_{2,x/y} e^{-j2k_{x/y} h_p}} \quad (4)$$

where $\tau_{1,x/y}$ and $\rho_{1,x/y}$ are the transmission and reflection coefficients of the first air and dielectric perforated disk interface, respectively, and $\tau_{2,x/y}$ and $\rho_{2,x/y}$ are the same parameters for the second dielectric-air interface, for the x - and y -directions, respectively. When the incident wave is linearly polarized, the amplitude of the transmitted wave through the perforated disk is equal in both the directions, while the $(\pi/2)$ phase difference is added to the transmitted waves. So, circular polarized transmitted waves can be generated. The dielectric perforated disk provides a phase shift and can control the dielectric properties of the incident wave to the lens. The height of the dielectric perforated disk is considered constant, and the wavenumber in the dielectric perforated disk is then adjusted to minimize the phase error between the desired and achieved transmission phases. In addition, changing the wavenumber of two axes, x and y , provides opportunities for developing circularly polarized radiation. An artificial dielectric structure is proposed in this work to adjust the wavenumber in the x - and y -directions to have an equal phase difference $\pm(\pi/2)$ and the desired phase shift in the direction of propagation. The equivalent dielectric constant along x - and y -axes (ϵ_x and ϵ_y) can be calculated by [11]

$$\epsilon_x = \left(\frac{q_{0-x}}{\epsilon_0} + \frac{q_{d-x}}{\epsilon_d} \right)^{-1}, \quad \epsilon_y = \left(\frac{q_{0-y}}{\epsilon_0} + \frac{q_{d-y}}{\epsilon_d} \right)^{-1} \quad (5)$$

where ϵ_0 and ϵ_d are the permittivities of the air and dielectric perforated disk, respectively. Moreover, q_0 and q_d are the fraction of the air and dielectric volume, respectively. The dielectric perforated disk consists of a structured arrangement of dielectric regions, as illustrated in Fig. 3. Each slab features a hole with dimensions denoted by c diameter and a and b dimensions in the x - and y -directions, respectively, while possessing a thickness h in the z -direction. The parameters a , b , c , and h determine the dielectric constant associated with each slab. Maintaining h as a constant value for all the slabs, the parameters a , b , and c serve as design

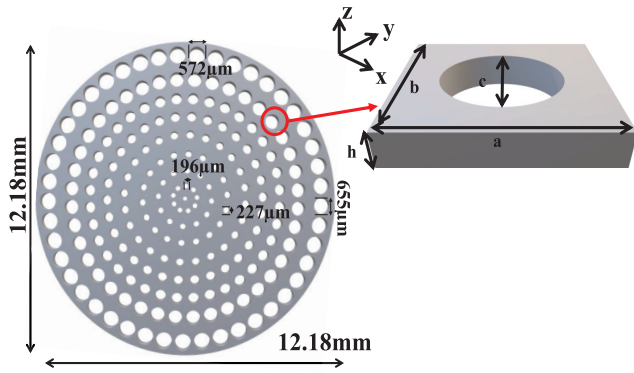
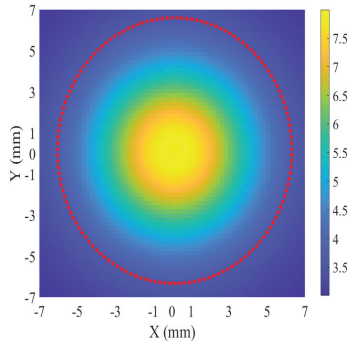


Fig. 3. Detailed geometry of the proposed dielectric perforated disk.


 Fig. 4. Desired distribution of dielectric constant for the dielectric perforated disk in the xy plane.

parameters crucial for ensuring the optimal required phase shift. The results of the synthesized calculations are presented in Fig. 3, which was created using MATLAB code to figure out the optimal size for each hole on the dielectric perforated disk. The combination of dielectric perforated disk and Fresnel zone lens enables controlling the wavenumber of the incident wave from feed to the lens, improving the lens' focusing potential and the antenna's gain. Furthermore, a desired phase shift between two axes is guaranteed with the anisotropic configuration of dielectric properties in the x - and y -directions. The distributed dielectric properties are developed in this dielectric perforated disk with circular holes with different dimensions. As illustrated in Fig. 3, the hole size increases as the distance from the center of the perforated disk grows. This implies that the dielectric perforated disk introduces additional delays for rays with shorter distances between the feed and the perforated disk, while rays with longer distances experience lower delays, as is shown in Fig. 4. Following this principle, all the propagated rays from the feed align in a constructive condition after passing through the dielectric perforated disk. The transition from dielectric strips [8] to the perforated disk significantly enhances performance by enabling a controlled spatial phase delay. Unlike the strip-based design, which introduces phase nonuniformities limiting gain, the perforated disk acts as a GRIN transition, optimizing phase correction and improving aperture efficiency. This modification leads to better impedance matching, reduced aberrations, and a more uniform wavefront, resulting in a gain improvement beyond the expected 3.7 dB due to size scaling.

C. GRIN Fresnel Zone Lens

These two components are constructed within a single silicon wafer, with one side housing the Fresnel lens and the other side featuring the GRIN dielectric perforated disk. This unified structure eliminates assembly and alignment losses or errors. As shown in Fig. 5, the antenna structure is mounted on a standard WM-380

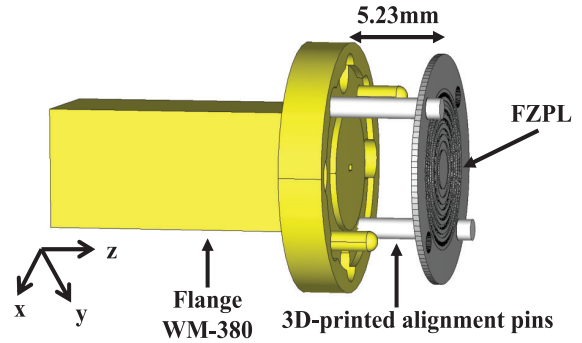


Fig. 5. Computer-aided design (CAD) model of the modified FZPL mounted on a standard WM-380 (WR-1.5) waveguide flange.

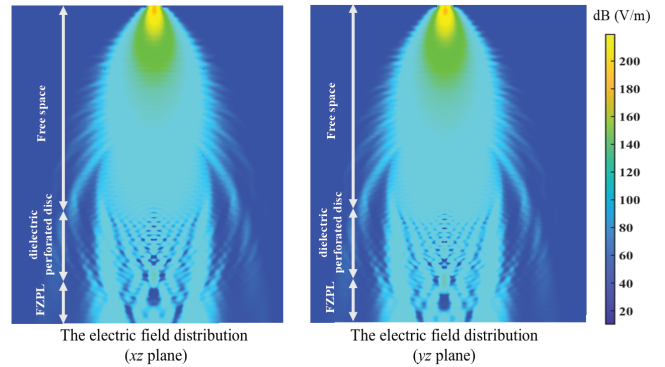
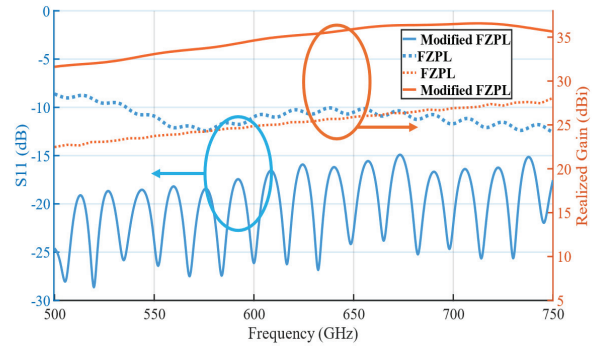

 Fig. 6. Simulated magnitude of electric field distribution in xz and yz cuts.


Fig. 7. Comparison of the simulated realized gain and return loss of FZPL and modified FZPL.

that uses two circular holes to ensure flange-to-chip alignment. The alignment pin used in this study follows the specifications detailed in our previous work [8]. The electromagnetic simulations and optimizations for the antenna design were performed using the commercial program CST Studio Suite. In Fig. 6, the simulated magnitude of the electric field distribution in xz and yz cuts demonstrates the spherical wave before the lens and the plane wave after the lens. To illustrate the impact of this innovative GRIN structure, we compare the return loss and realized gain of a conventional Fresnel zone lens with 13 zones to the modified Fresnel zone lens antenna of the same size and number of zones, differing only in the addition of the GRIN. The return loss in Fig. 7 reveals that the conventional Fresnel lens lacks satisfactory matching, exhibiting a return loss close to -10 dB across the entire band, an insufficient value. Conversely, including the dielectric perforated disk enhances the antenna bandwidth, enabling the modified Fresnel lens to cover the entire frequency band with

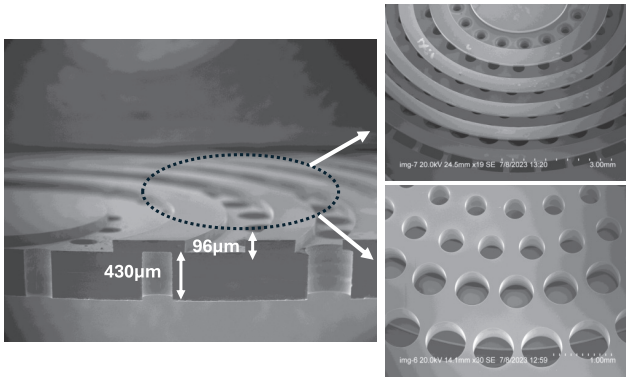


Fig. 8. SEM images of the manufactured FZPL antenna. Overall view of zone rings and cylindrical hollows of the dielectric perforated disk.

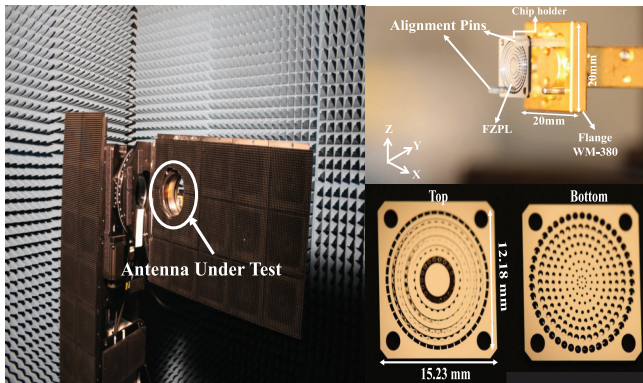


Fig. 9. Radiation pattern measurement setup at KTH THz Lab.

a return loss better than -15 dB. Furthermore, Fig. 7 shows that the realized gain is more than 36.6 dBi when the modified FZPL is mounted on the waveguide, while the realized gain of the FZPL is around 28.5 dBi.

III. FABRICATION

The fabrication process used for this study is based on a silicon-on-insulator (SOI) wafer configuration comprising silicon layers, the device layer, and the handle layer, separated by a $1\text{-}\mu\text{m}$ -thick buried oxide (BOX) layer. The device layer and the handle layer thickness are selected at 96 and $430\ \mu\text{m}$, respectively, with a resistivity of $2000\ \Omega\text{-cm}$, which is sufficient to minimize dielectric loss. Notably, the proposed fabrication process remains consistent with that outlined in [8], where a similar approach was adopted to develop the fabrication process for a Fresnel lens and dielectric perforated disk in the device and handle layers, respectively. Fig. 8 provides a close-up view from the side of two layers. As depicted in Fig. 8, the fabricated chips exhibit excellent condition based on the observed details. The fabrication incorporates four circular holes, as shown in Fig. 8, to facilitate the evaluation of the antenna's performance for left-hand circular polarization (LHCP). Due to the symmetrical shape of the lens and perforated disk, these holes enable the rotation of the antenna around the z -axis by 90° , allowing for effective testing of both the polarization states. However, in this communication, only one polarization state is measured for simplicity.

IV. MEASUREMENT

The realized gain, reflection loss, axial ratio (AR), and circular radiation pattern were measured in the THz anechoic chamber at KTH University, Sweden. The experimental setup comprises a three-axis azimuth, elevation, and polarization stage, with the antenna under

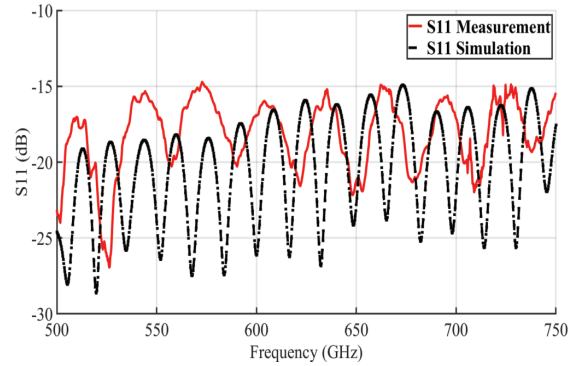


Fig. 10. Measured and simulated reflections for the modified FZPL antenna.

test (AUT) positioned at the center of rotation. The transmitting antenna for this arrangement is a high-gain horn antenna produced by Anteral. It is placed at a precise distance of 1.6 m from the AUT, ensuring optimal direct illumination. The received power is measured while scanning the AUT using two VDI frequency extenders powered by a ZVA-24 VNA. Fig. 9 displays a picture of the configuration. Furthermore, the fabricated lens antenna is visually represented in Fig. 9. A customized 3-D printed cylindrical alignment pin [8] with graduated radii has been devised and integrated to maintain the perfect alignment between the complex lens structure and the waveguide's feeding port, as illustrated in Fig. 9. This innovative solution enhances alignment accuracy, maintaining a nominal distance of 5.23 mm to the feeding port, thereby ensuring that the F/D ratio aligns with the nominal value. The measured return loss of the fabricated lens antenna is compared with the simulated data and illustrated in Fig. 10. The results indicate that the measured return loss of the lens antenna is consistently better than 15 dB across the frequency range from 500 to 750 GHz, representing a 40% FBW. Notably, the measured results closely align with the simulated data, demonstrating excellent agreement for the lens antenna. The differences in waveguide flange shape (circular versus square) and the fabricated lens boundary (square versus circular) have minimal impact on the antenna's performance. The primary factor contributing to the slight variations in S_{11} is fabrication tolerance, which is particularly critical at THz frequencies. However, a slight discrepancy in the period of the reflections between the measured S_{11} and simulations is observed. This difference is likely due to fabrication tolerances and material property variations, particularly at high frequencies, which can introduce minor differences in the physical structure not fully captured in the simulation models. Despite these variations, they do not significantly limit the overall performance of the antenna. The radiation pattern cuts of the FZPL antenna are shown in Fig. 11. The radiation patterns that exhibit circular polarization are observed in the xz and yz planes at three specific frequency points, namely, 500 , 625 , and 750 GHz. The comparison between the measured results and simulated data reveals excellent agreement for the lens antenna. Furthermore, the radiation pattern consistently maintains its profile and uniformity across the entire operating bandwidth. The antenna's measured and simulated realized gain is shown in Fig. 12(a), and the measured realized gain for the FPZL antenna is between 31.7 and 35.9 dBi, showing a maximum 0.9 -dB deviation from the simulation. In addition, the observed differences between the measured and simulated realized gains determine the level of antenna efficiency. This study examines radiation efficiency, which shows how well the antenna turns input power into radiated power. The simulation finds an average radiation efficiency of -0.73 dB, while the measured radiation efficiency is -1.05 dB. In addition, aperture efficiency is important in Fig. 12(b), which measures how well the aperture area works compared with its size. The simulation results show a maximum aperture efficiency of 58.8% , slightly better than the measured value of 54.23% . The consistent match between

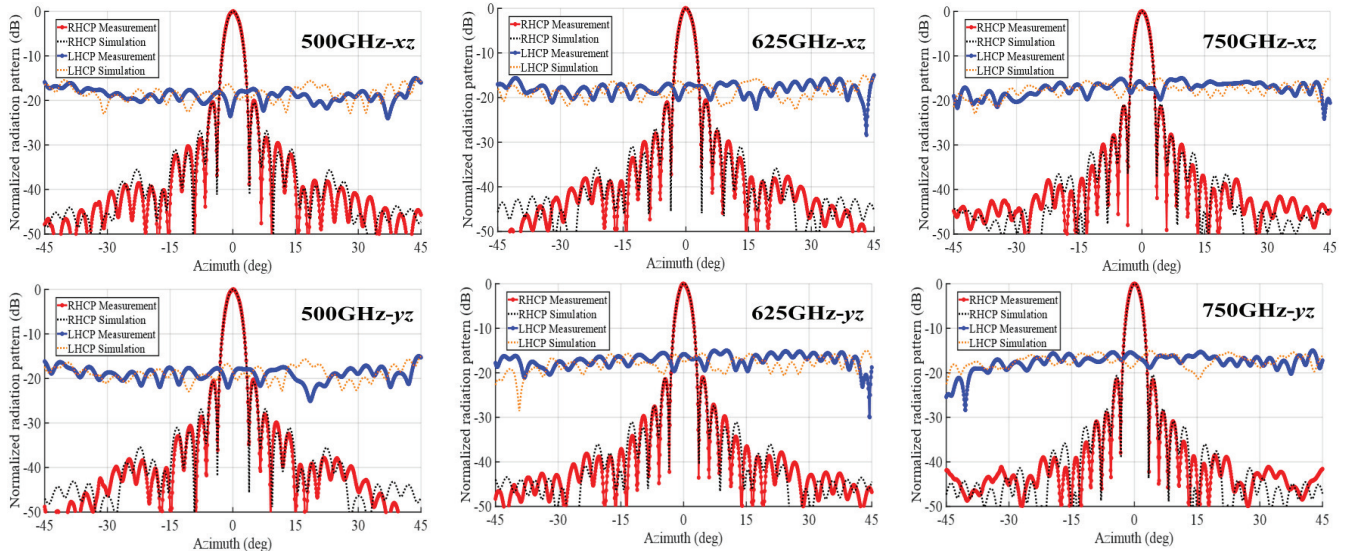


Fig. 11. Measured and simulated circular radiation patterns for the FZPL antenna.

TABLE I
COMPARISON OF THE THZ AND SUB-THZ HIGH-GAIN ANTENNAS

Reference	Topology	Frequency range (FBW*)	Maximum Gain (dBi)	Polarization	Maximum Aperture Efficiency (%)	Axial Ratio (dB)	Fabrication Technology
[22]	Spline diagonal Horn	500-750 GHz, 40% FBW	21.7	Linear	84	—	CNC-milling
[23]	Corrugated Horn	500-750 GHz, 40% FBW	34.5	Linear	—	—	Stacked rings
[24]	Quasi-Optical dual reflector	325-500 GHz, 43% FBW	32	Linear	44.2	—	CNC-milling
[14]	Dielectric Hemispherical Lens	230-310GHz, 30% FBW	30	Linear	39.5	—	CNC-milling
[11]	Dielectric perforated disc Lens	270-320GHz, 18.8% FBW	30.8	Circular	15.4	3	3D Printing
[5]	Dielectric Hemispherical Lens	1800-2100 GHz, 15.3% FBW	41.2	Linear	60	—	Silicon Micromachining
[25]	Dielectric hyperbolic silicon lens	450-550 GHz, 20% FBW	50	Linear	80	—	Silicon Micromachining
[6]	Flat array corporate feed	320-400GHz, 22% FBW	38	Linear	27.6	—	Silicon Micromachining
[8]	Elliptical Fresnel Lens	500-750GHz, 40% FBW	25.7	Circular	15	2.5	Silicon Micromachining
This Work	Graded index Fresnel lens	500-750GHz, 40% FBW	35.9	Circular	54.23	2.8	Silicon Micromachining

*Fractional Bandwidth based on return loss below -10dB.

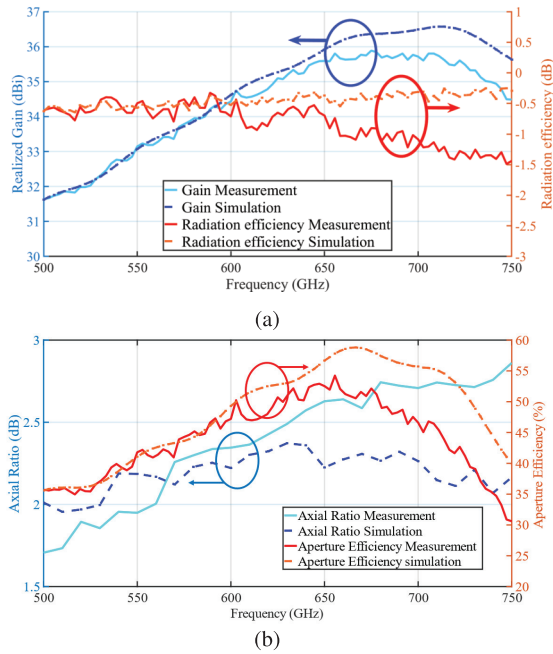


Fig. 12. Characterizing the performances of the FZPL antenna prototype compared with the simulated values. (a) Realized gain and radiation efficiency. (b) AR and aperture efficiency.

simulation and experiment indicates the good radiation and aperture efficiency of the antenna. Remarkably, these findings place this lens

antenna marginally better than other high-gain antennas in this range [6], [8] and in a highly good condition relative to other lens antennas at THz frequencies [13], [19]. The AR for the different frequencies is calculated to prove the circular polarization performance of the antenna. To calculate the AR, the main beam direction of the antenna is considered, and it is shown in Fig. 12(b) for the total bandwidth. The range of the AR is between 1.95 and 2.35 for simulation, and the measured values are between 1.7 and 2.8. The AR comparison demonstrates that the fabricated antenna agrees with the simulation. The AR of the GRIN Fresnel lens antenna is similar to that of the circularly polarized THz antennas discussed in [11] and [21], despite its broader bandwidth and higher operating frequency. Antennas reported at the sub-THz and THz frequencies are compared in Table I. Above 300 GHz, high-gain lens antennas are scarce, with only a limited number of reported designs [13], [25], [26]. The lens antenna in our study stands out as the first of its kind, boasting a gain of approximately 36 dBi in a compact size. It is also the only published antenna to achieve full-band performance and is one of the very few operating above 600 GHz, with exceptions noted in [8] and [5].

V. CONCLUSION

This communication introduces a novel antenna design operating in the 500–750-GHz range, using a modified FZPL to achieve a wide bandwidth and high gain in the sub-THz region. The utilization of silicon micromachining in the production of low-profile antennas represents a significant technological progression characterized by its outstanding performance characteristics, including high gain, circular polarization, and compact dimensions. Assuring about 36-dBi realized gain and circular polarization with a planar shape, it is the first full-band lens antenna at sub-THz frequencies. The measurements of the manufactured prototypes and simulation data agreed well,

especially when it came to radiation patterns and overall efficiency. This study contributes to understanding antenna technology in the sub-THz region, demonstrating the feasibility of practical applications requiring wide bandwidth, high gain, and compact designs.

REFERENCES

- [1] J. Gao et al., "Fast three-dimensional image reconstruction of a stand-off screening system in the terahertz regime," *IEEE Trans. THz Sci. Technol.*, vol. 8, no. 1, pp. 38–51, Jan. 2018.
- [2] P. Hillger, J. Grzyb, R. Jain, and U. R. Pfeiffer, "Terahertz imaging and sensing applications with silicon-based technologies," *IEEE Trans. THz Sci. Technol.*, vol. 9, no. 1, pp. 1–19, Jan. 2019.
- [3] A. Karimi, U. Shah, A. Madannejad, and J. Oberhammer, "Silicon-micromachined subterahertz frequency beam-steered dual-port array antenna," *IEEE Trans. Terahertz Sci. Technol.*, vol. 14, no. 2, pp. 258–268, Mar. 2024.
- [4] B. Zhang et al., "Metallic 3-D printed antennas for millimeter- and submillimeter wave applications," *IEEE Trans. Terahertz Sci. Technol.*, vol. 6, no. 4, pp. 592–600, Jul. 2016.
- [5] M. Alonso-delPino, T. Reck, C. Jung-Kubiak, C. Lee, and G. Chattopadhyay, "Development of silicon micromachined microlens antennas at 1.9 THz," *IEEE Trans. THz Sci. Technol.*, vol. 7, no. 2, pp. 191–198, Mar. 2017.
- [6] A. Gomez-Torrent et al., "A 38 dB gain, low-loss, flat array antenna for 320–400 GHz enabled by silicon-on-insulator micromachining," *IEEE Trans. Antennas Propag.*, vol. 68, no. 6, pp. 4450–4458, Jun. 2020.
- [7] A. Gomez-Torrent, "A low-profile and high-gain frequency beam steering subterahertz antenna enabled by silicon micromachining," *IEEE Trans. Antennas Propag.*, vol. 68, no. 2, pp. 672–682, Feb. 2020.
- [8] A. Madannejad, M. M. Gohari, U. Shah, and J. Oberhammer, "High-gain circularly polarized 500–750 GHz lens antenna enabled by silicon micromachining," *IEEE Trans. Antennas Propag.*, vol. 72, no. 5, pp. 4077–4085, May 2024.
- [9] Z.-C. Hao, J. Wang, Q. Yuan, and W. Hong, "Development of a low-cost THz metallic lens antenna," *IEEE Antennas Wireless Propag. Lett.*, vol. 16, pp. 1751–1754, 2017.
- [10] K. Liu, C. Zhao, S.-W. Qu, Y. Chen, J. Hu, and S. Yang, "A 3D-printed multibeam spherical lens antenna with ultrawide-angle coverage," *IEEE Antennas Wireless Propag. Lett.*, vol. 20, no. 3, pp. 411–415, Mar. 2021.
- [11] G. B. Wu, Y. S. Zeng, K. F. Chan, S. W. Qu, and C. H. Chan, "3-D printed circularly polarized modified Fresnel lens operating at terahertz frequencies," *IEEE Trans. Antennas Propag.*, vol. 67, no. 7, pp. 4429–4437, Jul. 2019.
- [12] M. S. Li, R. T. Ako, S. Sriram, C. Fumeaux, and W. Withayachumnankul, "Terahertz planar cavity antenna based on effective medium for wireless communications," *IEEE Trans. Terahertz Sci. Technol.*, vol. 14, no. 2, pp. 248–257, Mar. 2024.
- [13] M. Alonso-Delpino, S. Bosma, C. Jung-Kubiak, J. Bueno, G. Chattopadhyay, and N. Llombart, "A transmit lens array with high-gain and beam-steering capabilities at submillimeter wavelengths," *IEEE Trans. Terahertz Sci. Technol.*, vol. 14, no. 1, pp. 64–75, Jan. 2024.
- [14] K. Konstantinidis et al., "Low-THz dielectric lens antenna with integrated waveguide feed," *IEEE Trans. THz Sci. Technol.*, vol. 7, no. 5, pp. 572–581, Sep. 2017.
- [15] M. M. Gohari, O. Glubokov, S. Yu, and J. Oberhammer, "On-chip integration of orthogonal subsystems enabled by broadband twist at 220–325 GHz," *IEEE Trans. Microw. Theory Techn.*, vol. 71, no. 9, pp. 3929–3936, Sep. 2023.
- [16] B. Beuerle, J. Campion, U. Shah, and J. Oberhammer, "A very low loss 220–325 GHz silicon micromachined waveguide technology," *IEEE Trans. THz Sci. Technol.*, vol. 8, no. 2, pp. 248–250, Mar. 2018.
- [17] X. Zhao, U. Shah, O. Glubokov, and J. Oberhammer, "Micromachined subterahertz waveguide-integrated phase shifter utilizing supermode propagation," *IEEE Trans. Microw. Theory Techn.*, vol. 69, no. 7, pp. 3219–3227, Jul. 2021.
- [18] U. Shah et al., "A 500–750 GHz RF MEMS waveguide switch," *IEEE Trans. THz Sci. Technol.*, vol. 7, no. 3, pp. 326–334, May 2017.
- [19] M. Alonso-delPino, C. Jung-Kubiak, T. Reck, N. Llombart, and G. Chattopadhyay, "Beam scanning of silicon lens antennas using integrated piezomotors at submillimeter wavelengths," *IEEE Trans. THz Sci. Technol.*, vol. 9, no. 1, pp. 47–54, Jan. 2019.
- [20] IEEE Standard Test Procedures for Antennas, IEEE Standard Std 149-1979, 1979, pp. 1–144.
- [21] G. B. Wu, Y.-S. Zeng, K. F. Chan, S.-W. Qu, and C. H. Chan, "High-gain circularly polarized lens antenna for terahertz applications," *IEEE Antennas Wireless Propag. Lett.*, vol. 18, pp. 921–925, 2019.
- [22] H. J. Gibson, B. Thomas, L. Rolo, M. C. Wiedner, A. E. Maestrini, and P. de Maagt, "A novel spline-profile diagonal horn suitable for integration into THz split-block components," *IEEE Trans. Terahertz Sci. Technol.*, vol. 7, no. 6, pp. 657–663, Nov. 2017.
- [23] B. Maffei et al., "High-performance WR-1.5 corrugated horn based on stacked rings," *Proc. SPIE*, vol. 9153, pp. 91532W-1–91532W-9, Jul. 2014.
- [24] K. Fan, Z.-C. Hao, Q. Yuan, and W. Hong, "Development of a high gain 325–500 GHz antenna using quasi-planar reflectors," *IEEE Trans. Antennas Propag.*, vol. 65, no. 7, pp. 3384–3391, Jul. 2017.
- [25] S. van Berkel, M. Alonso-Delpino, C. Jung-Kubiak, and G. Chattopadhyay, "An $f/0.27$ high-gain lens antenna for ultrasmall platforms at THz frequencies," *IEEE Trans. Terahertz Sci. Technol.*, vol. 13, no. 5, pp. 549–560, Sep. 2023.
- [26] A. Bhutani, J. Dittmer, L. Valenziano, and T. Zwick, "Sub-THz conformal lens integrated WR3.4 antenna for high-gain beam-steering," *IEEE Open J. Antennas Propag.*, vol. 5, pp. 1306–1319, 2024.